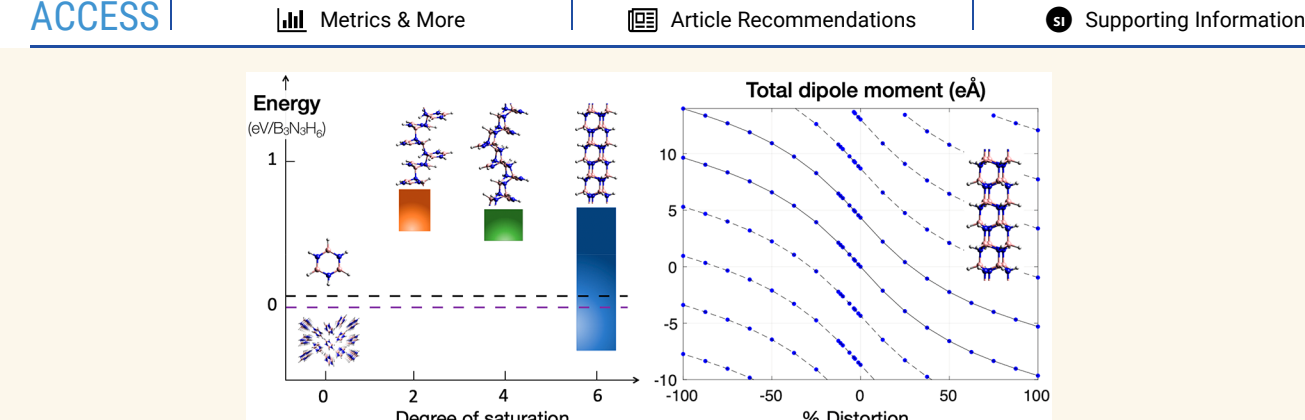
www.acsnano.org

# Theory of Borazine-Derived Nanothreads: Enumeration, Reaction Pathways, and Piezoelectricity

Tao Wang,\* En-Shi Xu, Bo Chen, Roald Hoffmann, and Vincent H. Crespi\*





ABSTRACT: Nanothreads are one-dimensional macromolecules formed by pressure-induced polymerization along stacks of multiply unsaturated (or highly strained) molecules such as benzene (or cubane). Borazine is isoelectronic to benzene yet with substantial bond polarity, thus motivating a theoretical examination of borazine-derived nanothreads with degrees of saturation of 2, 4, and 6 (defined as the number of four-coordinated boron and nitrogen atoms per borazine formula unit). The energy increases upon going from molecular borazine to degree-2 borazine-derived threads and then decreases for degree-4 and degree-6 nanothreads as more  $\sigma$  bonds are formed. With the constraint of no more than two borazine formula units within the repeat unit of the framework's bonding topology, there are only 13 fully saturated (i.e., degree-6) borazine-derived nanothreads that avoid energetically costly homopolar bonds (as compared to more than 50 such candidates for benzene-derived threads). Only two of these are more stable than borazine. Hypothetical pathways from molecular borazine to these two degree-6 borazine-derived nanothreads are discussed. This relative paucity of outcomes may assist in kinetic control of reaction products. Beyond the high mechanical strength also predicted for carbon-based threads, properties such as piezoelectricity and flexoelectricity may be accessible to the polar lattice of borazine-derived nanothreads, with intriguing prospects for expression in these extremely thin yet rigid objects.

KEYWORDS: Borazine, Nanothread, Topology Enumeration, Piezoelectricity, Flexoelectricity, Density Functional Theory

# **INTRODUCTION**

Downloaded via PENNSYLVANIA STATE UNIV on October 31, 2022 at 17:14:07 (UTC). See https://pubs.acs.org/sharingguidelines for options on how to legitimately share published articles.

Nanothreads are one-dimensional covalently bonded materials, with all "backbone" bonds saturated in the organic sense, the first of which was made from polymerization of benzene in the solid state. Nanothreads are thicker than conventional hydrocarbon polymers such as polyethylene and thinner than traditional nanowires: as ladder polymers, they are examples of the thinnest possible rigid objects. Nanothreads generally form by pressure-induced room-temperature polymerization of multiply unsaturated molecules along stacks in certain crystallographic directions of the parent molecular crystal. They have been synthesized from benzene 1,2 and pyridine,3 with evidence 4,5 of

both fully saturated ("degree-6") and two-thirds saturated ("degree-4") threads. Synthesis of aniline nanothreads under pressure at elevated temperatures has also been reported.8 Possible structures of nanothreads derived from monosubsti-

Received: March 21, 2022
Accepted: September 12, 2022
Published: September 27, 2022





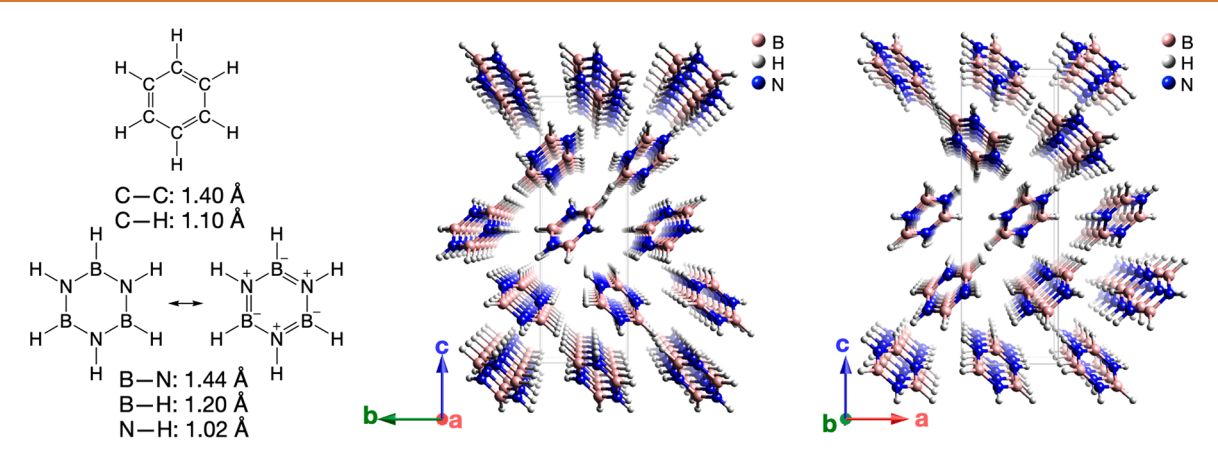


Figure 1. Molecular structures of benzene and borazine and the low-temperature crystal structure of borazine viewed along the a and b axes. Nanothreads formed from carbon-based precursors likely form by polymerization along such stacks.

tuted benzene<sup>9</sup> and polyaromatic hydrocarbons<sup>10</sup> have also been investigated. Recently, nanothreads were also synthesized from thiophene,<sup>11</sup> cubane,<sup>12</sup> furan,<sup>13</sup> azobenezene,<sup>14</sup> naphthalene-octafluoronaphthalene cocrystal,<sup>15</sup> and a phenol-pentafluorophenol cocrystal.<sup>16</sup> The success in synthesizing nanothreads from diverse organic precursors reveals a great variety of structures and functionalities that may be accessible through choice of precursor molecule or cocrystal.

All nanothreads explored to date have carbon-based backbones. Are inorganic nanothreads possible? One possible approach here would be to replace all carbon dimers with BN pairs, thus yielding an isoelectronic BN-based nanothread; this strategy follows a logic productive in the sp² world wherein carbon nanotubes motivated the synthesis of their boron nitride siblings<sup>17</sup> and wherein hexagonal boron nitride (h-BN) sheets support important applications as insulating layers in multilayer 2D electronics. <sup>18</sup> There is also a rich chemistry for BN analogues of all-C molecules. <sup>19</sup>

Borazine  $(B_3N_3H_6)$ , Figure 1) or "inorganic benzene" is isostructural and isoelectronic to benzene. As benzene forms organic nanothreads under pressure, one may anticipate that borazine can form BN nanothreads. The large difference in electronegativity between boron and nitrogen produces an uneven distribution of  $\pi$  electron density that favors nitrogen. This nonuniform  $\pi$  system reduces aromaticity<sup>20–22</sup> and makes borazine more reactive than benzene: it gradually loses hydrogen and polymerizes in the liquid state at room temperature<sup>23</sup> (in comparison, benzene decomposes at ~500 °C<sup>24</sup>). In the context of pressure-induced solid-state synthesis, one anticipates that borazine may initiate polymerization at a lower pressure than benzene does, due to the reduced aromaticity.<sup>13</sup>

At atmospheric pressure, borazine freezes at -58 °C into a tetragonal lattice with four molecules per unit cell.<sup>25</sup> Slipped stacking of borazine molecules, similar to that in benzene phase II (space group  $P2_1/c$ ),  $^{26,27}$  is evident along a and b lattice directions, while no closely spaced molecular stacks are seen along c (Figure 1, middle and right panels). The closest contacts (B···N vs C···C) in the a and b stacks of the P=1 atm structures are  $\sim$ 0.3 Å longer for borazine, as compared to a benzene crystal. The polymerization under pressure may afford borazine nanothreads along one of these stacking directions; possible such structural outcomes are enumerated here. Borazine does polymerize at ambient pressure and relatively low temperature (70 °C), with loss of H, into polymers of not precisely

characterized structure.<sup>28,29</sup> These are not the nanothreads we study. In addition to the high mechanical strength<sup>30,31</sup> and anisotropic thermal conductivity<sup>32</sup> anticipated for carbon nanothreads, borazine nanothreads may also possess interesting electromechanical properties due to the heteropolar nature of the BN lattice in a highly anisotropic nanoscale structure with an unusually stiff backbone.

#### **RESULTS AND DISCUSSION**

Bond Connectivity/Topology: The Range of Possibilities. Borazine-derived nanothreads should have a bond connectivity similar to their benzene-derived analogues, as both precursor molecules have six-membered rings. However, there is a choice between heteropolar (B-N) and homopolar (B-B, N-N) bonds between adjacent borazine molecules in the polymers that is absent for carbon. Simple electrostatic reasoning favors B-N over B-B or N-N. Since any deviation from a fully heteropolar bipartite three-fold coordinate BN framework (at 1:1 B/N stoichiometry) can be decomposed into B⇔N swaps, and each such swap inverts the hetero/homopolar character of six bonds (i.e., from 0 to 6 homopolar bonds starting from a perfect lattice, or  $1 \Leftrightarrow 5$ ,  $2 \Leftrightarrow 4$ ,  $3 \Leftrightarrow 3$  such bonds for swaps in nonideal lattices), every such framework (including a nanothread) must have an even number of homopolar bonds. Homopolar B-B/N-N bonds in a 1:1 stoichiometric degree-6 borazine-derived nanothread must therefore appear in pairs.

Structures with B–B/N–N bonds are energetically unfavorable compared with those having only B–N bonds. A test using isomers of BN analogues of cyclobutane and cyclohexane (see Figure S1) shows that each pair of B–B/N–N bonds imposes a large energetic penalty of  $\sim$ 4.0 eV (i.e., such isomers are  $\sim$ 4.0 eV higher in energy than isomers with only B–N bonds). Therefore, borazine nanothreads with homopolar bonds are excluded in our enumeration; this excludes all BN nanothreads with odd-membered rings.

We follow the convention of previous work in categorizing nanothreads based on the degree of saturation, i.e. the average number of sp³ carbons (or borons + nitrogens) in each progenitor six-membered ring² (more precisely, per six C or BN atoms). Unreacted benzene or borazine is degree-0 while fully saturated threads are degree-6. We enumerate BN threads of degrees-2, -4, and -6 and adopt the naming convention from the previous work² with the format of "Roman numeral—Arabic numeral", where the Roman numeral represents the degree of saturation, and the Arabic numeral labels topologically distinct

structure. If a structure has conformers, a Latin alphabet letter will be added after the Arabic number to distinguish them. Strictly speaking, we should also label structures as C or BN-based; e.g., CVI-1, BNVI-2. The extra labels confuse the discussion, so we drop the atom designation, as it is usually clear in context.

Among the 50 previously enumerated degree-6 benzenederived nanothreads<sup>6</sup> (lowest in energy for C) there are 13 with only even-membered rings. The BN analogues, VI-1 to VI-13, are shown in Figure S2. Five of these 13 structures have three polymerization bonds in each direction from every progenitor borazine, and eight have two bonds up and four down the column. Only two of these BN nanothread candidates, VI-1 and VI-2, contain only hexagonal rings. Benzene-derived nanothreads VI-1 and VI-2, previously called "tube (3,0)" and "tube (2,1)", are the hydrogenated sp<sup>3</sup> analogues of the (3,0) and (2,1) carbon nanotubes. We avoid that notation here to avoid confusion with nanotubes and instead call them "thread (3,0)" and "thread (2,1)", or VI-1 and VI-2, respectively. VI-2 has also been called "polytwistane" since the structure is an extension of the twistane molecule. By the naming convention of Xu et al., the two thread structures have also been labeled as 123456 and 143652, which indicate clearly the connection pattern between adjacent molecules.

Imposing the heteropolarity rule (only B–N bonds allowed) on the 23 previously proposed degree-4 carbon nanothreads yields only 10 BN nanothreads (illustrated in Figure S3). IV-12 spontaneously relaxes to the fully saturated structure VI-1 since the two closest B···N contacts (2.30 and 2.45 Å) are within the reaction distance to form two new  $\sigma$  bonds between the adjacent borazine rings. Prior enumerations of degree-4 carbon threads did not consider four-fold rings; adding these to the BN system yields 19 additional candidate structures. The reason for including four-fold rings in the BN system is that they are much less strained and are more competitive in energy to six-fold rings than one obtains for C. The matter is probed numerically in the Supporting Information, where the relative energies of representative C and BN model molecules are compared in Figure S4.

For degree-2 threads, all previously enumerated structures can be converted to BN analogues without homopolar bonds due to the weak topological constraints in these sparsely connected systems (Figure S5). However, family II-1 falls apart into borazine, and families II-6 and II-7 also have a few members that fall apart.

In the prior enumeration for carbon-based threads, <sup>6,7</sup> all degree-3 and degree-5 threads and a fraction of degree-2 and degree-4 threads were excluded due to the existence of radicals (structures with one dangling bond) and diradicals (two dangling bonds, such as those arising from the degree-4 and degree-2 building blocks shown in the top row of Figure 2). However, for BN threads, these structures simply host three-coordinate borons and nitrogens, as illustrated in Figure 2, bottom row. The expansion of enumeration to include these additional "diradical" or "radical" structures will be reported in due course.

Most carbon nanothread bond topologies can be notionally converted directly to BN threads within their original unit cells, but certain cases (such as VI-13) require unit cell doubling to avoid homopolar bonds at the interface between cells. Thus, all BN threads examined here have either two or four borazine formula units in their topological unit cells (i.e., the cell that

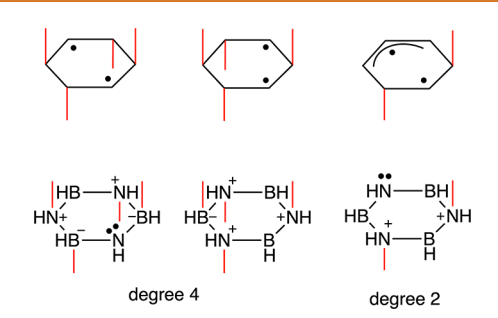


Figure 2. Diradical building blocks of benzene nanothreads (top row) and the similar, but nondiradical, building blocks of borazine nanothreads (bottom row).

contains the repeat of the bond connectivity, regardless of precise atomic coordinates).

Structural Energetics. The energy ranges for BN threads with different degrees of saturation are shown in Figure 3. Going from degree-0 borazine to degree-2 BN threads, the energy increases; as more bonds are formed in degree-4 and degree-6 threads, the system becomes more stable. A similar trend is seen in benzene-derived nanothreads.7 The nonmonotonicity originates from two competing effects: aromaticity stabilizes degree-0 (even if it is less for BN than C), while additional  $\sigma$  bonds stabilize degree-6, with the summit at degree-2 constituting an intrinsic barrier against nanothread formation at ambient pressure. What is different from the benzene system is that only two BN nanothreads—threads VI-1 and VI-2—are found to be more stable than molecular borazine, whereas more than 15 carbon nanothreads were calculated to be more stable than benzene. This derives from a  $\pi$  to  $\sigma$  bond conversion (what happens in increasing the degree of saturation in a polymer) being roughly twice as stabilizing for C as for BN and the greater viability of structures with five-membered rings for C. The DFT PBE level calculations show that the reaction energy of three molecules of ethylene to cyclohexane is -3.43 eV (the experimental reaction enthalpy is -2.86 eV calculated from NIST Chemistry WebBook https://webbook.nist.gov/ chemistry/), while that of three BH<sub>2</sub>NH<sub>2</sub> to an analogous cyclohexane structure is only -2.08 eV.

The relaxed structures of the four lowest-energy degree-6 BN threads in our enumeration are shown in the top row of Figure 4; the remainder can be found in Figure S2. Threads VI-1 and VI-2 are the only structures that contain solely six-membered rings, and as anticipated, they are the two lowest-energy degree-6 BN threads, respectively, 0.23 and 0.21 eV per borazine formula unit more stable than solid-state molecular borazine (see below). They are 0.32 and 0.30 eV per borazine more stable than the gasphase molecule. In the carbon thread analogue, the energetic order of these two threads is reversed: VI-1 (called "tube(3,0)" in the previous work<sup>6</sup>) is 0.16 eV/(CH)<sub>6</sub> less stable than VI-2 (called "polytwistane" in the previous work<sup>6</sup>) presumably due to unfavorable H···H eclipsing between adjacent six-membered rings along the thread in the carbon analogue. Those unfavorable H···H interactions may actually become attractive "dihydrogen bonding" in the BN thread.<sup>33</sup>

In general, dihydrogen bonding has been invoked as an attractive interaction between two hydrogens that are attached to very electropositive and very electronegative atoms, respectively. These may occur (and be variously rationalized) with either an electrostatic interaction or a  $\sigma$  bond donor (X–H bonds, where X = O, N, C, halogen) to  $\sigma^*$  bond acceptor (M–H bonds, where M = B, Al, Ga, Ir, Mo, Mn, Os, Re, Ru, W)

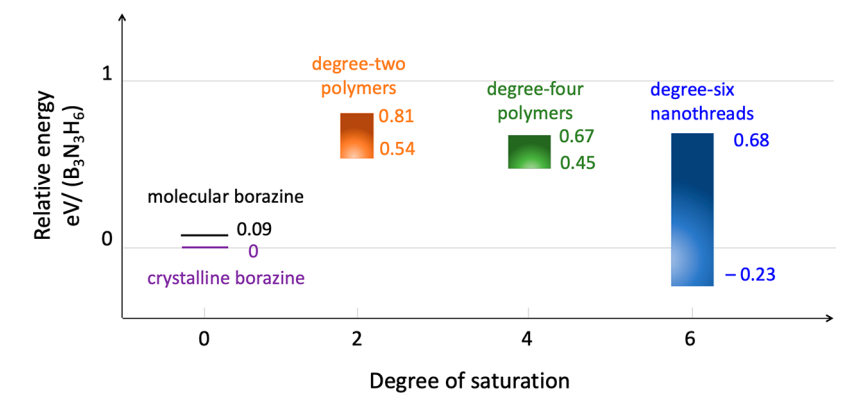


Figure 3. Calculated energies of borazine nanothreads with different degrees of saturation relative to atmospheric-pressure low-temperature crystalline borazine, in units of eV per  $B_3N_3H_6$ . Only fully saturated species are more stable than the precursor crystal, although enthalpic effects at high pressure will tilt this landscape.

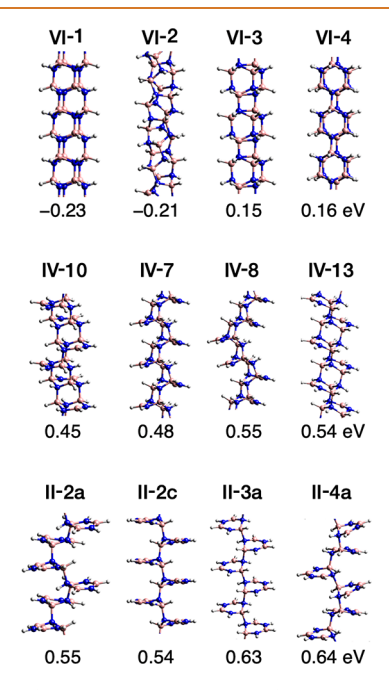


Figure 4. Four lowest-energy BN nanothread structures of each degree of saturation: 2, 4, and 6, referenced to the energy of a molecular crystal of borazine. Only VI-1 and VI-2, composed entirely of six-fold rings, have a negative formation energy at atmospheric pressure.

donation, as shown in Figure 5 (left). The typical dihydrogen bonding H···H contact is 1.7–2.2 Å and the XH···H—M angle is

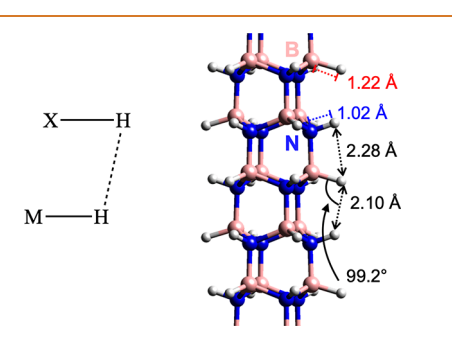


Figure 5. Sketch of the dihydrogen bond (left) and the dihydrogen bond in BN thread VI-1 with H···H contact distance of 2.10 Å and NH···H-B angle of 99.2°.

90–135°. <sup>34</sup> For BN thread VI-1, the corresponding H···H distance is 2.10 Å and the NH···H—B angle is 99.2°. The bonds involved optimize to BH and NH, 1.22 and 1.02 Å, respectively (Figure 5 right).

Dihydrogen bonding also exists in BN threads VI-3, VI-4, VI-5, VI-6, VI-10, VI-11, and VI-12 with B-H and N-H bond lengths and H $\cdot$  H contacts in range of 1.21-1.23, 1.01-1.03, and 1.84-2.20 Å, respectively. Similar interactions raise the melting point of ammonia borane (H $_3$ NBH $_3$ ) to be 284 °C higher than that of its hydrocarbon analogue ethane. It is worth noting that the potential of interchain dihydrogen bonds could influence BN thread packing, which might lead to denser packing than that for benzene-derived nanothreads.

Square/octagon-containing BN nanothreads are from 0.38 to 0.91 eV per borazine formula unit less stable than VI-1. The B–N bonds in all degree-6 BN nanothreads are generally close to 1.58 Å, similar to those in cubic BN and ammonia borane, and longer than those in borazine, 1.44 Å. B–H and N–H bonds are similarly close in length ( $\sim$ 1.22 and  $\sim$ 1.02 Å, respectively) to those in borazine<sup>23</sup> (1.20 and 1.02 Å, respectively) and ammonia borane<sup>35</sup> (1.216 and 1.014 Å, respectively). The bond lengths of both B–H and N–H in the degree-6 BN thread structures with dihydrogen bonds do not change significantly compared with those for structures without dihydrogen bonds.

Turning to the partially saturated degree-4 and degree-2 threads (the four lowest-energy structures are in the lower rows of Figure 4, and the complete sets of structures are shown in Figures S3 and S5), the spread in energies for the degree-4 BN nanothreads (0.45 to 0.67 eV per borazine formula unit) is close to that for carbon threads (0.58 to 0.72 eV per benzene formula unit) without consideration of structures with separated three-coordinated B or N atoms (analogues of carbon "diradicals"). For degree-2 BN nanothreads, the energy range is from 0.54 to 0.81 eV per borazine formula unit. The total and relative energies (to crystal borazine) for each enumerated BN threads are provided in the Supporting Information.

Nanothreads IV-10 and IV-13 introduce still another feature specific to BN nanothreads, namely, B—H···B and N—H···N hydrogen bonding. The left and middle panels of Figure 6 reproduce these two structures, marking the bonds involved in red ovals. These interactions derive in a way from "unhooking" the double bond in a B—N unit and viewing the electron pair as localized according to the inherent electronegativity, as in the aminoborane structure shown in the right panel of Figure 6. N—H···N hydrogen bonds are a routine phenomenon in

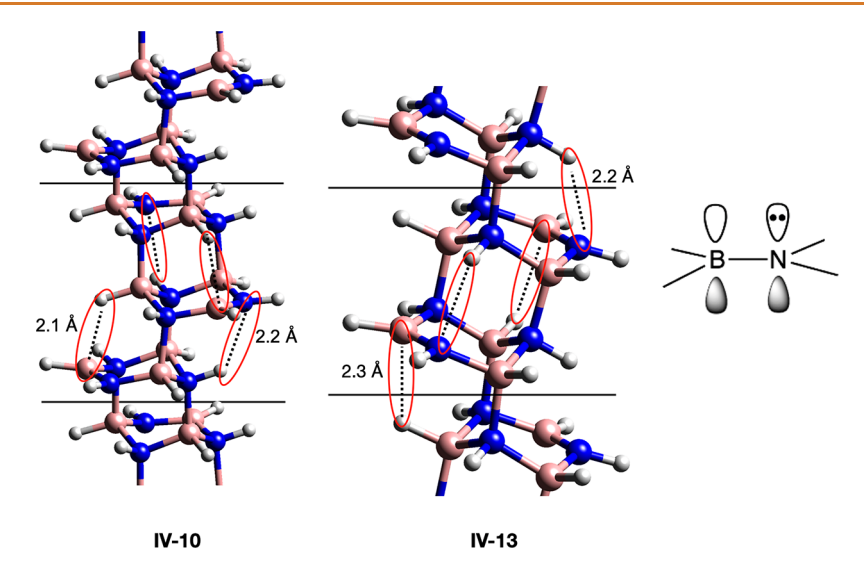


Figure 6. Structures of degree-4 BN threads IV-10 (left) and IV-13 (middle). The B—H···B and N—H···N hydrogen bonds involved are marked in the red ovals with the H···B and H···N contacts connected by the dotted lines. The corresponding hydrogen bond lengths range from 2.1 to 2.3 Å. The localized electron pair in the aminoborane structure (right).

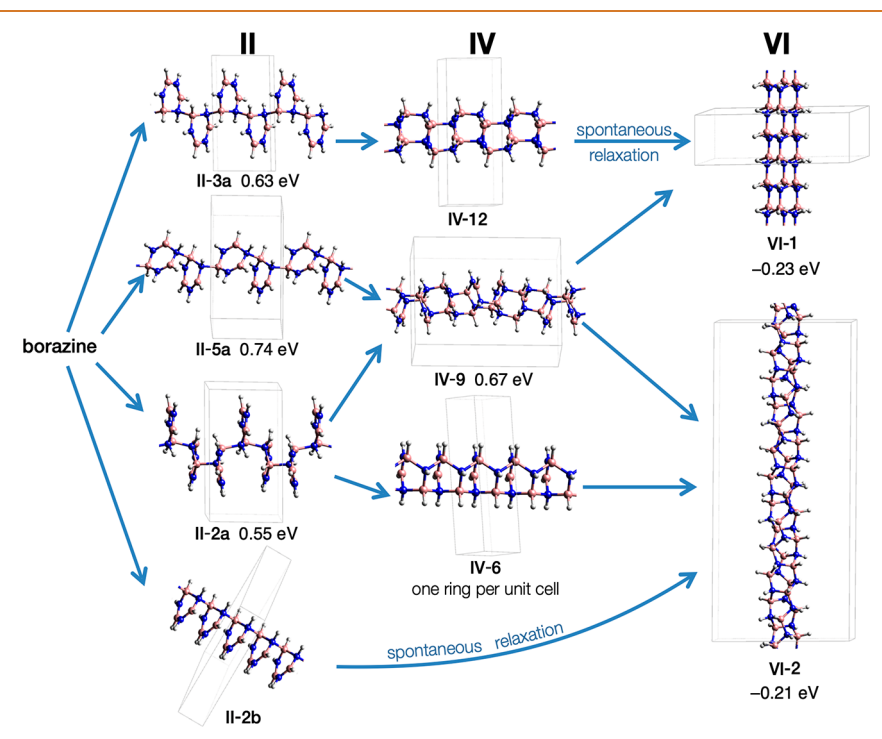


Figure 7. Hypothetical pathways from molecular borazine toward threads VI-1 and VI-2, the only BN nanothreads that are lower in energy than the precursor at ambient conditions. All energies are per borazine unit, relative to crystalline borazine calculated without van der Waals interactions. Structures II-2b and IV-12 spontaneously relax to the more saturated structures. Unit cells (periodic approximate for the helical VI-2) are marked.

chemistry;<sup>36</sup> they are electron-rich three-center bonds that occur in both bent and linear forms and are mostly asymmetrical.<sup>37</sup> The N···N distance in known hydrogen bonds typically ranges from 2.9 to 3.1 Å.<sup>38,39</sup> B–H···B entities are common in borane chemistry; these two-electron three-center electron-poor systems are mostly symmetrical and highly bent (note relationship to  ${\rm H_3}^+$ ). In nanothreads, the B–H···B distances are not symmetrical, due perhaps to the rigidity of the backbone preventing optimization of the B····B separation and the three-fold  $\sigma$  bonding of the hydrogen-bearing B to the surrounding nanothread backbone. The appearance of N–H···

N and the B-H···B bonding in pairs, i.e., sharing a B-N dimer, may be synergistic due to charge localization within the dimer.

In the structures where we encounter them, the H···B and H··· N contacts range from 2.1 to 2.3 Å, and the B–H···B and N–H··· N angles are 115-118 and  $\sim 127^{\circ}$ , respectively. The corresponding B–H and N–H bonds are elongated  $\sim 2$  and  $\sim 1\%$ , respectively, compared to those in borazine. The overall ranges of bond lengths for B–H and N–H in all degree-4 BN threads are 1.20-1.23 and 1.01-1.03 Å, respectively, which are almost the same as those in degree-6 BN threads and close to those in ammonia borane or borazine. Note also that structures

IV-10 and IV-13 place the residual B—N double bonds of each borazine far enough from each other (by either spiraling them around the thread axis or alternating them across the thread backbone in the so-called *anti* configuration<sup>7</sup>) that these structures may be plausible kinetic end points to thread backbone polymerization.

Expanding our view to include threads that contain four-fold and eight-fold rings, other interesting features emerge. The degree-4 thread IV-14 (see Figure S6) forms B-H-B multicenter bonds when relaxed at a 5.5% compressed axial lattice constant (i.e., 94.5% of the original axial lattice constant). Further interesting phenomena arise when periodic boundary conditions are relaxed: a degree-4 structure prefers a tightly curled geometry that can close up onto itself to form a wheel, illustrated in Figure S7. A few other degree-4 structures (Figure S8) have very loose spirals with large diameters that may require a different synthetic strategy because under high pressure they will not have access to enough reaction volume. In degree-2 BN nanothreads, the II-1 family of structures in which the atoms at the 1 and 4 positions on the ring bond up and down with neighbors (para configuration) automatically collapse into unbonded borazine molecules. We here defer our interests in all these intermediate structures and focus on the structures that are directly related to low-energy fully saturated nanothreads.

For purposes of comparisons between different thread backbones, we simply reference nanothread formation energies to the atmospheric-pressure low-temperature structure of borazine (i.e., below 215 K). We do not reference to the energy of the high-pressure crystal structure of borazine because it is experimentally unknown and also because actual enthalpies of thread formation at pressure would require calculations of densely packed thread lattices, which is beyond our current scope. The total energy of this molecular crystal is 0.09 eV per B<sub>3</sub>N<sub>3</sub>H<sub>6</sub> lower than that of gas-phase borazine, reflecting stabilizing dispersion and electrostatic force interactions. The closest intermolecular H···H distance is 2.54 Å (2.49 Å in experiment<sup>25</sup>), outside the hydrogen van der Waals sphere. Stacked molecular columns favor homopolar intermolecular closest approaches (i.e., intermolecular B···B and N···N are closer than B···N), consistent with higher multipoles dominating the electrostatics.

Hypothetical Reaction Pathways. Similar to the case of benzene, the complex isomerism of borazine nanothreads at different stages of saturation yields many potential reaction pathways from molecular borazine to nanothreads; a reasonable way to track these is to follow the increase in degree of saturation. Since only borazine threads VI-1 and VI-2 are more stable than the molecule at ambient conditions, we consider only sequences leading to these in Figure 7. The "pathways" shown there are more properly thought of as topological relationships that connect the molecule to degree-6 threads, as several of the intermediate structures shown are not metastable. More specifically, degree-2 II-2b and degree-4 IV-12 (following the naming convention of Chen et al. 7) spontaneously relax into more saturated structures (II-2b relaxes to VI-2 without any degree-4 intermediates, and IV-12 relaxes to VI-1), while structure IV-6, although it can locally relax in its original unit cell, spontaneously relaxes to thread VI-2 after cell doubling followed by a slight symmetry-lowering structural perturbation. Thread IV-9 is also barely metastable: axial compression by 1% converts it to VI-1 (and VI-2 may also be possible for a longer axial supercell). The optimal axial lattice constant for IV-9 is determined from a fit of the Birch-Murnaghan equation of

state where the IV-9 structure is retained (see Figure S9 right panel). The phonon spectra (Figure S10) for the threads in Figure 7 and other representative examples are provided in the Supporting Information with analysis for the vibrational modes and stabilities.

Taken as a whole, these results suggest that BN nanothread formation from borazine strongly favors a fully saturated degree-6 final state. As a caveat, note that pressure may favor certain metastable (e.g., degree-4) outcomes, especially if they place residual B=N double bonds at well-separated locations along the backbone, as noted above. Detailed consideration of reaction pathways under pressure in the solid state is beyond our scope here and awaits further information on the high-pressure phase diagram of crystalline borazine. To our knowledge, only the atmospheric-pressure crystal structure is known.<sup>25</sup>

**Properties.** As anticipated based on the strength of the B-N single bond, the VI-1 and VI-2 threads have very high Young's moduli (Table 1), 0.72 and 0.75 TPa, respectively, when the cross-sectional areas are defined as for benzene-derived nanothreads by dividing the linear (B, N) atom density of the nanothread by the volume per atom of cubic BN. These Young's moduli almost match those of the corresponding benzenederived nanothreads, although note that the nonlinear mechanical response of BN systems may differ from that of the carbon nanothreads, due to the energetic cost of any homopolar bonds which may come into play under plastic deformations. The Young's moduli for the other degree-6 BN threads are much lower, which might be due to internal strain associated with four-fold rings and the looser atomic packing of corresponding eight-fold rings. All of the enumerated degree-6 BN threads are predicted to be insulators with band gaps larger than 4.5 eV, as shown in Table 1.

Hexagonal BN sheets do not support a spontaneous electric dipole moment due to their three-fold symmetry. This symmetry is broken upon wrapping the sheet into a nanotube, yielding a spontaneous electric dipole when the nanotube's so-called "wrapping indices" (i.e., the circumference expressed in lattice coordinates (n,m)) satisfy (n-m) mod  $3 \neq 0$ . <sup>40</sup> In BN nanothreads, the sp³ geometry provides further symmetry breaking. A single BN thread VI-1 is calculated following the modern theory of polarization <sup>41</sup> to hold an axial moment of -9.64 electron·Å, following a single branch of the dipole lattice through an adiabatic pathway from a stack of borazine rings to a fully formed nanothread or its inverse, as shown in Figure 8a,b. Importantly, there are no metallic states along this adiabatic path (Figure S11).

If we assume that BN nanothreads pack into a near-hexagonal structure with  ${\sim}6.5$  Å lattice constant (similar to carbon threads) and consistent polarity, we obtain an estimated polarization density of  ${\sim}0.97$  C/m² for the bulk material, higher than that of polyvinylidene fluoride polymer (PVDF) ferroelectrics  $^{42}$  (0.178 C/m²) or BaTiO3 (0.27 C/m²).  $^{43}$  BN nanothreads are further distinguished from traditional polymer ferroelectrics by their exceptionally rigid backbones. Additional symmetry lowering through incorporation of heteroatoms or functional groups (for example, selective fluorination) may further enhance or reorient the polarization density.

In addition to a spontaneous electric dipole moment, sp<sup>2</sup> BN nanotubes also exhibit a piezoelectric response: 42,44 so-called zigzag BN nanotubes couple axial strain to an axial electric dipole, while armchair BN nanotubes couple an axial electric dipole to torsional strain. BN-based nanothreads that share lattice symmetry with their sp<sup>2</sup> nanotube cousins should exhibit

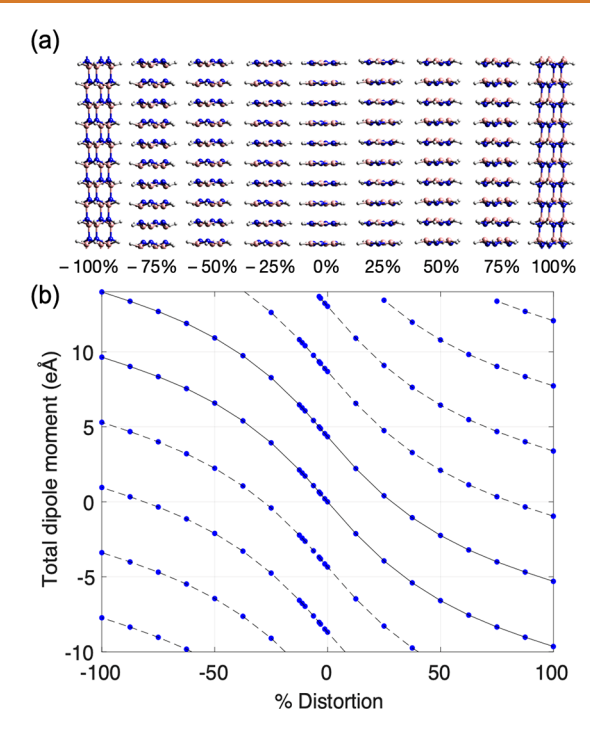


Figure 8. (a) Representative intermediates for evolution from a borazine stack to the degree-6 borazine thread VI-1 and its invert. (b) Calculated total dipole moment as a function of percent distortion from the molecular stack (0%) to the fully saturated thread VI-1(100% distortion) and its invert (-100% distortion). The blue dots are connected with solid and dashed lines to show branches of the polarization lattice.

similar types of coupling. BN thread VI-1 couples axial strain to axial dipole (as does BN thread VI-2, but more weakly). The piezoelectric stress tensor component that couples axial strain to axial dipole,  $e_{33}$ , and the piezoelectric strain coefficient  $d_{33}$  that couples stress to axial dipole are calculated by fitting the calculated polarization with respect to strain (Figure 9a) and stress (Figure 9b), with results shown in Table 1. The value of  $e_{33}$  for BN thread VI-1,  $0.86 \, \text{C/m}^2$ , is modest compared with that of commercial piezoelectric materials such as PbTiO<sub>3</sub> <sup>45,46</sup> (1–10 C/m²) but larger in magnitude than that of PVDF polymer and its copolymers <sup>47,48</sup> ( $-0.25 \, \text{to} -0.33 \, \text{C/m}^2$ ) and zigzag sp² boron nitride nanotubes <sup>42</sup> ( $0.18 \, \text{to} 0.39 \, \text{C/m}^2$ ), suggesting BN nanothreads as potential alternative materials for lead-free piezoelectric devices. <sup>49</sup>

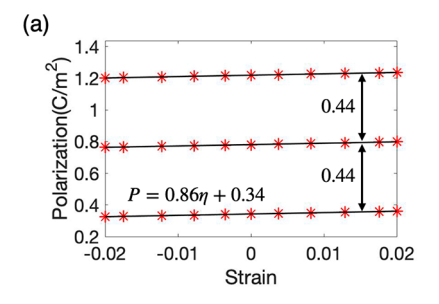
In contrast to the positive piezoelectric coefficients for VI-1, threads VI-2 and VI-3 yield negative piezoelectric coefficients comparable to that of PVDF. While the negative piezoelectric

Table 1. Calculated Physical Properties of the Four Lowest-Energy BN Degree-6 Nanothreads

	energy per B <sub>3</sub> N <sub>3</sub> H <sub>6</sub> (eV)	band gap (eV)	Young's modulus (TPa)	piezoelectric stress coefficient $e_{33}$ (C/m <sup>2</sup> )	piezoelectric strain coefficient $d_{33}$ (pm/V)
VI-1	-0.23	4.89	0.72	0.86	2.36
VI-2	-0.21	5.13	0.75	-0.34	-1.04
VI-3	0.15	4.70	0.48	-0.35	-1.42
VI-4	0.16	4.57	0.49	0	0

effect for PVDF and its copolymers ( $e_{33}$  from -0.25 to -0.33 C/m<sup>2</sup>) is thought to originate from electromechanical coupling between intermixed crystalline lamellae and amorphous regions,  $^{50,51}$  that for single-phase threads VI-2 and VI-3 may instead originate in the frozen-ion contribution to the piezoelectric response. The isolated thread VI-4 has a centrosymmetric structure and thus has no piezoelectric response along the thread axis. The piezoelectric strain coefficients  $d_{33}$  for all four degree-6 BN threads are smaller than those for common piezoelectric materials (-14.7 pm/V for BaTiO<sub>3</sub>,  $^{54}$  -49.6 pm/V for PVDF<sup>51</sup>) owing to their very high axial stiffness; this mechanical strength is of course an advantage in certain actuator applications.

The distinctive feature of polarization response in BN nanothreads does not relate to the simple magnitude of the polarization density or piezoelectric response but to the exceptional combination of narrowness, rigidity and reduced symmetry possible in nanothreads. This combination of qualities may allow uniform external fields to generate very large strain gradients transverse to the thread axis. Two scenarios are possible here: a gradient across a single low-symmetry thread, or a gradient across two or more distinct mechanically coupled (i.e., cross-linked) threads. For example, VI-1 and VI-2 threads have opposite signs to their longitudinal piezoelectric coefficients and thus could generate a very large strain gradient across the interface between them: a flexoelectric response. A similar effect is seen h-BN bilayers that have AA' stacking registry. 55 The naïve field-induced curvature  $\kappa$  (i.e., assuming no internal mechanical relaxations) is  $(d_{ii}^1 - d_{ii}^2)E/h$ , where h is the interthread/interlayer distance, E the external electric field, and  $d_{ii}^1$  and  $d_{ii}^2$  the piezoelectric strain coefficients of the two threads  $(d_{ii}^1 = d_{33}^{V_i^2-1}, d_{ii}^2 = d_{33}^{V_i-2})$  or h-BN layers  $(d_{ii}^1 = -d_{ii}^2 = d_{11})$ . Using  $h \sim$ 6.5 Å as the interthread separation yields  $\kappa \sim 0.0052$  E (measuring E in volt/meter), which is the same order of magnitude as that for a h-BN bilayer<sup>55</sup> ( $\kappa \sim 0.0089$  E). Both of these naive values would decrease modestly when allowing for full mechanical relaxation.



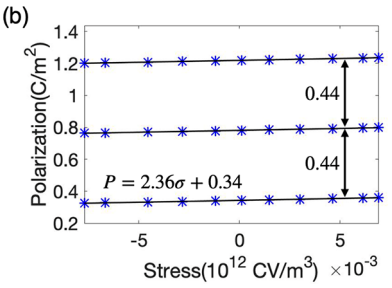


Figure 9. Calculated polarization versus (a) strain and (b) stress for BN thread VI-1; the identical slopes here indicate that the proper piezoelectric response is branch independent.

To generate a transverse displacement of ~150 nm in a beam  $\sim$ 20  $\mu$ m long requires similar fields in both systems: 0.084 V/ $\mu$ m for the h-BN bilayer<sup>55</sup> and 0.144 V/ $\mu$ m for coupled BN threads. In contrast, the pull-in field needed to achieve the same transverse displacement for a 20  $\mu m$  long few-layer graphene electro-mechanical beam is much larger,  $\sim$ 12 V/ $\mu$ m, due to the absence of intrinsic flexoelectric coupling. 55,56 Nanothreads which lack any rotational symmetry about the thread axis, such as VI-4 and VI-13 in Figure S2, may express similar couplings within a single thread wherein the characteristic dimension h is even smaller and the now-covalent mechanical coupling between the extensile and contractile regions is much stronger than is possible in van der Waals systems; such a thread may provide a monolithic flexoelectric actuator at the extreme limit of small size. Similar behavior may also be accessible to carbonbased nanothreads that host symmetry-lowering heteroatoms.

More generally, as piezoelectric response is often dominated by domain dynamics, structural anisotropy, mechanical moduli and physical size, the unusual structural organization of nanothreads into extremely anisotropic, dense lattices of very thin yet rigid symmetry-broken linear constituents conveys intriguing possibilities for exceptional expressions of electromechanical coupling at both the bulk and individual-thread scales.

## **CONCLUSION**

Borazine nanothreads with degrees of saturation of 2, 4, and 6 are enumerated using the same methods for benzene-derived nanothreads with the exclusion of homopolar bonds due to large energy penalty. With the constraint of only two borazine formula units per topological unit cell, there are only 13 fully saturated BN nanothreads, only two of which are more stable than the borazine molecules. Unlike partially saturated benzene nanothreads in which only degree-2 and degree-4 threads without radicals and diradicals are possible, degree-3, degree-5 and degree-2 and degree-4 could exist with normal threecoordinated borons and nitrogens. The polarization and piezoelectric response for the first four lowest-energy degree-6 BN threads are calculated theoretically. The piezoelectric stress coefficients for BN thread VI-(3,0), VI-(2,1), and VI-3 are modest compared with commercial bulk piezoelectric materials but larger than PVDF polymer and with a much larger modulus and distinct form of nanoscale organization that lends itself to the induction of very large transfer strain gradients, due to the unusual combination of extreme narrowness and rigidity possible in nanothreads.

## **METHODS**

The calculations for energies for BN nanothreads, borazine crystal, and gas-phase borazine molecule are performed with density functional theory, 57 with the projector-augmented wave (PAW) 58 method and the Perdew-Burke-Ernzerhof (PBE) generalized gradient approximation (GGA)<sup>59,60</sup> exchange-correlation energy functional as implemented in the Vienna Ab initio Simulation Package (VASP).61-65 All structures are optimized with an energy cutoff of 600 eV for the plane-wave basis, 0.05 eV Gaussian smearing, and the energy and force criteria of  $10^{-6} \text{ eV}$ and 0.01 eV/Å, respectively, without van der Waals correction. To avoid complications arising from threads packing densely into a crystal, here, we consider only isolated nanothreads in a  $a \times a \times c$  hexagonal unit cell with  $a \ge 11$  Å for separating the closest hydrogen pairs on neighboring threads. Atomic positions for BN threads are relaxed with a line of k points along the axial direction separated by less than 0.2  $Å^{-1}$ . The axial lattice constant was interpolated from the Birch-Murnaghan equation of state at a dense set of fixed axial cell lengths (see Supporting Information for details), and the final structure was rerelaxed at the optimal axial lattice constant. In the absence of information on the high-pressure crystal structure of borazine, the atmospheric-pressure low-temperature crystal structure provides a reference for energy comparison. This crystal structure is optimized with a 3  $\times$  3  $\times$  1 k points sampling for the unit cell. The gas-phase borazine molecule is relaxed in a cubic cell of 10 Å  $\times$  10 Å  $\times$  10 Å with gamma point sampled only. The computational details for Young's modulus and phonon spectra for BN nanothreads are provided in the Supporting Information.

The dipole moments from both ionic and electronic contributions for isolated BN threads are calculated using projector augmented waves and the PBE generalized gradient approximation exchange-correlation functional in VASP. To this end, the structural coordinates for the four lowest-energy fully saturated BN threads are further relaxed to a threshold of 1 meV/Å at an energy cutoff of 700 eV. Polarization in a periodic system is multivalued, i.e. it is a polarization lattice with equally spaced branches. The electronic polarization is calculated using the modern theory of polarization<sup>41</sup> as implemented in VASP. This method requires a nonpolar reference from which one obtains the change of polarization relative to the system of interest through an adiabatic process. We reference to a stack of borazine rings with the same interring distance as one of our enumerated threads (the "BN thread VI-1"), generating a series of intermediates through boron/nitrogen buckling of successive rings to build a pathway to a fully saturated BN thread. Here we only consider the dipole moment along the thread axis, i.e., p = $p_3$ . The polarization density is estimated for threads packed into a nearhexagonal structure with ~6.5 Å lattice constant similar to that for benzene-derived nanothreads.

The piezoelectric stress response  $e_{\alpha j}$  and strain response  $d_{\alpha j}$  are defined  $^{52,54}$  by

$$e_{\alpha j} = -\frac{\partial \sigma_{j}}{\partial \varepsilon_{\alpha}} \bigg|_{\eta} = \frac{\partial P_{\alpha}}{\partial \eta_{j}} \bigg|_{\varepsilon} \tag{1}$$

$$d_{aj} = -\frac{\partial \eta_j}{\partial \varepsilon_a} \bigg|_{\sigma} = \frac{\partial P_a}{\partial \sigma_j} \bigg|_{\varepsilon} \tag{2}$$

where P is the polarization,  $\varepsilon$  is the electric field,  $\eta$  is strain, and  $\sigma$  is stress. We consider the piezoelectric response that couples axial strain/stress to axial dipole, i.e.,  $e_{33}$  and  $d_{33}$ , by fitting the calculated polarization and stress for axial strains from -0.02 to 0.02 with optimized atomic positions. Although eqs 1 and 2 define the improper piezoelectric tensors, it is evident that  $e_{33}^{\text{improper}} = e_{33}^{\text{proper}}$  and  $d_{33}^{\text{improper}} = d_{33}^{\text{proper}}$  as the unit cell area in our calculations does not vary with strain/stress. Thus, the calculated  $e_{33}$  and  $d_{33}$  are independent of choice of branch and can be compared with experimental data that measures the current density flowing through the sample in response to a slow deformation (i.e., the proper piezoelectric response).

#### ASSOCIATED CONTENT

# Supporting Information

The Supporting Information is available free of charge at https://pubs.acs.org/doi/10.1021/acsnano.2c02778.

Calculated relative energies of isomers of BN analogues of cyclobutane and cyclohexane (Figure S1); strain comparison of several saturated cyclic hydrocarbons and their BN analogues (Figure S4); relaxed structures of the enumerated BN degree-6 (Figure S2), degree-4 (Figure S3), degree-2 (Figure S5) threads, and degree-4 IV-14 with a compressed lattice constant (Figure S6); degree-4 structures with a wheel shape (Figure S7) and large diameters/hollow cores (Figure S8); fit of the Birch—Murnaghan equation of state for structure IV-7 and IV-9 (Figure S9); calculated phonon spectra for BN nanothreads (Figure S10); band structures of BN nanothread

VI-1, its intermediates and inverse (Figure S11), and calculated energies, computational details, and vibrational analysis for BN nanothreads (PDF)

Atomic coordinates of the reported BN nanothreads, crystalline borazine, and gas-phase borazine (ZIP)

# **AUTHOR INFORMATION**

## **Corresponding Authors**

Tao Wang — Department of Physics, Pennsylvania State University, University Park, Pennsylvania 16802, United States; Present Address: Department of Mechanical Engineering, Pennsylvania State University, University Park, Pennsylvania 16802, United States; ◎ orcid.org/0000-0003-2833-1592; Email: tuw169@psu.edu

Vincent H. Crespi — Department of Physics, Department of Chemistry, and Department of Materials Science and Engineering, Pennsylvania State University, University Park, Pennsylvania 16802, United States; Materials Research Institute, Pennsylvania State University, University Park, Pennsylvania 16802, United States; orcid.org/0000-0003-3846-3193; Email: vhc2@psu.edu

#### **Authors**

En-Shi Xu — Department of Physics, Pennsylvania State University, University Park, Pennsylvania 16802, United States; School of Physics and Electronics, Qiannan Normal University for Nationalities, Duyun 558000, P.R. China; Materials Research Institute, Pennsylvania State University, University Park, Pennsylvania 16802, United States

Bo Chen — Donostia International Physics Center, 20018 Donostia-San Sebastian, Spain; IKERBASQUE, Basque Foundation for Science, 48009 Bilbao, Spain; orcid.org/ 0000-0002-5084-1321

Roald Hoffmann — Department of Chemistry and Chemical Biology, Cornell University, Ithaca, New York 14853-1301, United States; orcid.org/0000-0001-5369-6046

Complete contact information is available at: https://pubs.acs.org/10.1021/acsnano.2c02778

# **Author Contributions**

The manuscript was written through contributions of all authors. All authors have given approval to the final version of the manuscript.

#### Notes

The authors declare no competing financial interest.

## **ACKNOWLEDGMENTS**

This work is supported by the Center for Nanothread Chemistry (CNC), funded by the National Science Foundation (CHE-1832471).

## **REFERENCES**

- (1) Fitzgibbons, T. C.; Guthrie, M.; Xu, E.; Crespi, V. H.; Davidowski, S. K.; Cody, G. D.; Alem, N.; Badding, J. V. Benzene-Derived Carbon Nanothreads. *Nat. Mater.* **2015**, *14*, 43–47.
- (2) Li, X.; Baldini, M.; Wang, T.; Chen, B.; Xu, E.; Vermilyea, B.; Crespi, V. H.; Hoffmann, R.; Molaison, J. J.; Tulk, C. A.; Guthrie, M.; Sinogeikin, S.; Badding, J. V. Mechanochemical Synthesis of Carbon Nanothread Single Crystals. *J. Am. Chem. Soc.* **2017**, *139*, 16343–16349
- (3) Li, X.; Wang, T.; Duan, P.; Baldini, M.; Huang, H.-T.; Chen, B.; Juhl, S. J.; Koeplinger, D.; Crespi, V. H.; Schmidt-Rohr, K.; Hoffmann, R.; Alem, N.; Guthrie, M.; Zhang, X.; Badding, J. V. Carbon Nitride

- Nanothread Crystals Derived from Pyridine. J. Am. Chem. Soc. 2018, 140, 4969-4972.
- (4) Duan, P.; Li, X.; Wang, T.; Chen, B.; Juhl, S. J.; Koeplinger, D.; Crespi, V. H.; Badding, J. V.; Schmidt-Rohr, K. The Chemical Structure of Carbon Nanothreads Analyzed by Advanced Solid-State NMR. *J. Am. Chem. Soc.* **2018**, *140*, 7658–7666.
- (5) Wang, T.; Duan, P.; Xu, E.-S.; Vermilyea, B.; Chen, B.; Li, X.; Badding, J. V.; Schmidt-Rohr, K.; Crespi, V. H. Constraining Carbon Nanothread Structures by Experimental and Calculated Nuclear Magnetic Resonance Spectra. *Nano Lett.* **2018**, *18*, 4934–4942.
- (6) Xu, E.; Lammert, P. E.; Crespi, V. H. Systematic Enumeration of Sp3 Nanothreads. *Nano Lett.* **2015**, *15*, 5124–5130.
- (7) Chen, B.; Hoffmann, R.; Ashcroft, N. W.; Badding, J.; Xu, E.; Crespi, V. Linearly Polymerized Benzene Arrays As Intermediates, Tracing Pathways to Carbon Nanothreads. *J. Am. Chem. Soc.* **2015**, *137*, 14373–14386.
- (8) Nobrega, M. M.; Teixeira-Neto, E.; Cairns, A. B.; Temperini, M. L. A.; Bini, R. One-Dimensional Diamondoid Polyaniline-like Nanothreads from Compressed Crystal Aniline. *Chem. Sci.* **2018**, *9*, 254–260
- (9) Silveira, J. F. R. V.; Muniz, A. R. Functionalized Diamond Nanothreads from Benzene Derivatives. *Phys. Chem. Chem. Phys.* **2017**, 19, 7132–7137.
- (10) Demingos, P. G.; Muniz, A. R. Carbon Nanothreads from Polycyclic Aromatic Hydrocarbon Molecules. *Carbon* **2018**, *140*, 644–652
- (11) Biswas, A.; Ward, M. D.; Wang, T.; Zhu, L.; Huang, H.-T.; Badding, J. V.; Crespi, V. H.; Strobel, T. A. Evidence for Orientational Order in Nanothreads Derived from Thiophene. *J. Phys. Chem. Lett.* **2019**, *10*, 7164–7171.
- (12) Huang, H.-T.; Zhu, L.; Ward, M. D.; Wang, T.; Chen, B.; Chaloux, B. L.; Wang, Q.; Biswas, A.; Gray, J. L.; Kuei, B.; Cody, G. D.; Epshteyn, A.; Crespi, V. H.; Badding, J. V.; Strobel, T. A. Nanoarchitecture through Strained Molecules: Cubane-Derived Scaffolds and the Smallest Carbon Nanothreads. *J. Am. Chem. Soc.* 2020, 142, 17944–17955.
- (13) Huss, S.; Wu, S.; Chen, B.; Wang, T.; Gerthoffer, M. C.; Ryan, D. J.; Smith, S. E.; Crespi, V. H.; Badding, J. V.; Elacqua, E. Scalable Synthesis of Crystalline One-Dimensional Carbon Nanothreads through Modest-Pressure Polymerization of Furan. *ACS Nano* **2021**, *15*, 4134–4143.
- (14) Romi, S.; Fanetti, S.; Alabarse, F.; Mio, A. M.; Bini, R. Synthesis of Double Core Chromophore-Functionalized Nanothreads by Compressing Azobenzene in a Diamond Anvil Cell. *Chem. Sci.* **2021**, 12, 7048–7057.
- (15) Ward, M. D.; Tang, W. S.; Zhu, L.; Popov, D.; Cody, G. D.; Strobel, T. A. Controlled Single-Crystalline Polymerization of C10H8-C10F8 under Pressure. *Macromolecules* **2019**, *52*, 7557–7563.
- (16) Gerthoffer, M. C.; Wu, S.; Chen, B.; Wang, T.; Huss, S.; Oburn, S. M.; Crespi, V. H.; Badding, J. V.; Elacqua, E. 'Sacrificial' Supramolecular Assembly and Pressure-Induced Polymerization: Toward Sequence-Defined Functionalized Nanothreads. *Chem. Sci.* **2020**, *11*, 11419–11424.
- (17) Chopra, N. G.; Luyken, R. J.; Cherrey, K.; Crespi, V. H.; Cohen, M. L.; Louie, S. G.; Zettl, A. Boron Nitride Nanotubes. *Science* **1995**, 269, 966–967.
- (18) Novoselov, K. S.; Mishchenko, A.; Carvalho, A.; Castro Neto, A. H. 2D Materials and van Der Waals Heterostructures. *Science* **2016**, 353, aac9439.
- (19) Pichierri, F. Boron-Nitrogen Analogues of Cyclo[18]Carbon. Chem. Phys. Lett. 2020, 738, 136860.
- (20) Kiran, B.; Phukan, A. K.; Jemmis, E. D. Is Borazine Aromatic? Unusual Parallel Behavior between Hydrocarbons and Corresponding B–N Analogues. *Inorg. Chem.* **2001**, *40*, 3615–3618.
- (21) Shen, W.; Li, M.; Li, Y.; Wang, S. Theoretical Study of Borazine and Its Derivatives. *Inorg. Chim. Acta* **2007**, *360*, 619–624.
- (22) Islas, R.; Chamorro, E.; Robles, J.; Heine, T.; Santos, J. C.; Merino, G. Borazine: To Be or Not to Be Aromatic. *Struct. Chem.* **2007**, *18* (6), 833–839.

- (23) Hohnstedt, L. F.; Schaeffer, G. W. Borazine Chemistry. *Borax to Boranes*; Advances in Chemistry; American Chemical Society: Washington, DC, 1961; Vol. 32, pp 232–240.
- (24) Zanetti, J. E.; Egloff, G. The Thermal Decomposition of Benzene. *J. Ind. Eng. Chem.* **1917**, *9*, 350–356.
- (25) Boese, R.; Maulitz, A. H.; Stellberg, P. Solid-State Borazine: Does It Deserve to Be Entiteled "Inorganic Benzene"? *Chem. Ber.* **1994**, *127*, 1887–1889.
- (26) Piermarini, G. J.; Mighell, A. D.; Weir, C. E.; Block, S. Crystal Structure of Benzene II at 25 Kilobars. *Science* 1969, 165, 1250–1255.
- (27) Wen, X.-D.; Hoffmann, R.; Ashcroft, N. W. Benzene under High Pressure: A Story of Molecular Crystals Transforming to Saturated Networks, with a Possible Intermediate Metallic Phase. *J. Am. Chem. Soc.* **2011**, *133*, 9023–9035.
- (28) Fazen, P. J.; Beck, J. S.; Lynch, A. T.; Remsen, E. E.; Sneddon, L. G. Thermally Induced Borazine Dehydropolymerization Reactions. Synthesis and Ceramic Conversion Reactions of a New High-Yield Polymeric Precursor to Boron Nitride. *Chem. Mater.* **1990**, *2*, 96–97.
- (29) Fazen, P. J.; Remsen, E. E.; Beck, J. S.; Carroll, P. J.; McGhie, A. R.; Sneddon, L. G. Synthesis, Properties, and Ceramic Conversion Reactions of Polyborazylene. A High-Yield Polymeric Precursor to Boron Nitride. *Chem. Mater.* **1995**, *7*, 1942–1956.
- (30) Roman, R. E.; Kwan, K.; Cranford, S. W. Mechanical Properties and Defect Sensitivity of Diamond Nanothreads. *Nano Lett.* **2015**, *15*, 1585–1590.
- (31) Silveira, J. F. R. V.; Muniz, A. R. Diamond Nanothread-Based 2D and 3D Materials: Diamond Nanomeshes and Nanofoams. *Carbon* **2018**, *139*, 789–800.
- (32) Zhan, H.; Zhang, G.; Zhang, Y.; Tan, V. B. C.; Bell, J. M.; Gu, Y. Thermal Conductivity of a New Carbon Nanotube Analog: The Diamond Nanothread. *Carbon* **2016**, *98*, 232–237.
- (33) Verma, K.; Viswanathan, K. S. The Borazine Dimer: The Case of a Dihydrogen Bond Competing with a Classical Hydrogen Bond. *Phys. Chem. Chem. Phys.* **2017**, *19*, 19067–19074.
- (34) Custelcean, R.; Jackson, J. E. Dihydrogen Bonding: Structures, Energetics, and Dynamics. *Chem. Rev.* **2001**, *101*, 1963–1980.
- (35) Thorne, L. R.; Suenram, R. D.; Lovas, F. J. Microwave Spectrum, Torsional Barrier, and Structure of BH3NH3. *J. Chem. Phys.* **1983**, 78, 167–171.
- (36) Katrusiak, A. Stereochemistry and Transformations of NH—N Hydrogen Bonds Part I. Structural Preferences for the Hydrogen Site. *J. Mol. Struct.* **1999**, 474, 125–133.
- (37) Perrin, C. L.; Ohta, B. K. Symmetry of NHN Hydrogen Bonds in Solutiong. *J. Mol. Struct.* **2003**, *644*, 1–12.
- (38) Prasad, N.; Govil, G. Study of Geometrical Parameters in N-H··· N Type of Hydrogen Bonds. *Proc. Indian Acad. Sci.* **1980**, 89, 253–262.
- (39) Steiner, T. Lengthening of the N–H Bond in N–H ··· N Hydrogen Bonds. Preliminary Structural Data and Implications of the Bond Valence Concept. *J. Chem. Soc. Chem. Commun.* **1995**, *13*, 1331–1332
- (40) Mele, E. J.; Král, P. Electric Polarization of Heteropolar Nanotubes as a Geometric Phase. *Phys. Rev. Lett.* **2002**, *88*, 056803.
- (41) King-Smith, R. D.; Vanderbilt, D. Theory of Polarization of Crystalline Solids. *Phys. Rev. B* **1993**, *47*, 1651–1654.
- (42) Nakhmanson, S. M.; Nardelli, M. B.; Bernholc, J. Ab Initio Studies of Polarization and Piezoelectricity in Vinylidene Fluoride and BN-Based Polymers. *Phys. Rev. Lett.* **2004**, *92*, 115504.
- (43) Mirseraji, M.; Shahraki, M. G. DFT Study of the Polarization Behaviors of Various Distorted Barium Titanate Crystals: The Role of Atomic Displacements. *Phys. B Condens. Matter* **2018**, 538, 120–130.
- (44) Sai, N.; Mele, E. J. Microscopic Theory for Nanotube Piezoelectricity. *Phys. Rev. B* **2003**, *68*, 241405.
- (45) Sághi-Szabó, G.; Cohen, R. E.; Krakauer, H. First-Principles Study of Piezoelectricity in PbTiO3. *Phys. Rev. Lett.* **1998**, *80*, 4321–4324.
- (46) Sághi-Szabó, G.; Cohen, R. E.; Krakauer, H. First-Principles Study of Piezoelectricity in Tetragonal PbTiO 3 and PbZr 1/2 Ti 1/2 O 3. *Phys. Rev. B* **1999**, *59*, 12771–12776.

- (47) Tashiro, K.; Kobayashi, M.; Tadokoro, H.; Fukada, E. Calculation of Elastic and Piezoelectric Constants of Polymer Crystals by a Point Charge Model: Application to Poly(Vinylidene Fluoride) Form I. *Macromolecules* **1980**, *13*, 691–698.
- (48) Carbeck, J. D.; Rutledge, G. C. Temperature Dependent Elastic, Piezoelectric and Pyroelectric Properties of  $\beta$ -Poly(Vinylidene Fluoride) from Molecular Simulation. *Polymer* **1996**, *37*, 5089–5097.
- (49) Wei, H.; Wang, H.; Xia, Y.; Cui, D.; Shi, Y.; Dong, M.; Liu, C.; Ding, T.; Zhang, J.; Ma, Y.; Wang, N.; Wang, Z.; Sun, Y.; Wei, R.; Guo, Z. An Overview of Lead-Free Piezoelectric Materials and Devices. *J. Mater. Chem. C* 2018, 6, 12446–12467.
- (50) Katsouras, I.; Asadi, K.; Li, M.; van Driel, T. B.; Kjær, K. S.; Zhao, D.; Lenz, T.; Gu, Y.; Blom, P. W. M.; Damjanovic, D.; Nielsen, M. M.; de Leeuw, D. M. The Negative Piezoelectric Effect of the Ferroelectric Polymer Poly(Vinylidene Fluoride). *Nat. Mater.* **2016**, *15*, 78–84.
- (51) Soin, N.; Boyer, D.; Prashanthi, K.; Sharma, S.; Narasimulu, A. A.; Luo, J.; Shah, T. H.; Siores, E.; Thundat, T. Exclusive Self-Aligned  $\beta$ -Phase PVDF Films with Abnormal Piezoelectric Coefficient Prepared via Phase Inversion. *Chem. Commun.* **2015**, *51*, 8257–8260.
- (52) Kim, J.; Rabe, K. M.; Vanderbilt, D. Negative Piezoelectric Response of van Der Waals Layered Bismuth Tellurohalides. *Phys. Rev. B* **2019**, *100*, 104115.
- (53) Liu, S.; Cohen, R. E. Origin of Negative Longitudinal Piezoelectric Effect. *Phys. Rev. Lett.* **2017**, *119*, 207601.
- (54) Wu, X.; Vanderbilt, D.; Hamann, D. R. Systematic Treatment of Displacements, Strains, and Electric Fields in Density-Functional Perturbation Theory. *Phys. Rev. B* **2005**, *72*, 035105.
- (55) Duerloo, K.-A. N.; Reed, E. J. Flexural Electromechanical Coupling: A Nanoscale Emergent Property of Boron Nitride Bilayers. *Nano Lett.* **2013**, *13*, 1681–1686.
- (56) Kim, S. M.; Song, E. B.; Lee, S.; Seo, S.; Seo, D. H.; Hwang, Y.; Candler, R.; Wang, K. L. Suspended Few-Layer Graphene Beam Electromechanical Switch with Abrupt on-off Characteristics and Minimal Leakage Current. *Appl. Phys. Lett.* **2011**, *99*, 023103.
- (57) Kohn, W.; Sham, L. J. Self-Consistent Equations Including Exchange and Correlation Effects. *Phys. Rev.* **1965**, *140*, A1133–A1138.
- (\$8) Blöchl, P. E. Projector Augmented-Wave Method. *Phys. Rev. B* **1994**, *50*, 17953–17979.
- (59) Perdew, J. P.; Burke, K.; Ernzerhof, M. Generalized Gradient Approximation Made Simple. *Phys. Rev. Lett.* **1996**, *77*, 3865–3868.
- (60) Perdew, J. P.; Yue, W. Accurate and Simple Density Functional for the Electronic Exchange Energy: Generalized Gradient Approximation. *Phys. Rev. B* **1986**, *33*, 8800–8802.
- (61) Kresse, G.; Hafner, J. Ab Initio Molecular Dynamics for Liquid Metals. *Phys. Rev. B* **1993**, *47*, 558–561.
- (62) Kresse, G.; Furthmüller, J.; Hafner, J. Theory of the Crystal Structures of Selenium and Tellurium: The Effect of Generalized-Gradient Corrections to the Local-Density Approximation. *Phys. Rev. B* **1994**, *50*, 13181–13185.
- (63) Kresse, G.; Furthmüller, J. Efficient Iterative Schemes for Ab Initio Total-Energy Calculations Using a Plane-Wave Basis Set. *Phys. Rev. B* **1996**, *54*, 11169–11186.
- (64) Kresse, G.; Furthmüller, J. Efficiency of Ab-Initio Total Energy Calculations for Metals and Semiconductors Using a Plane-Wave Basis Set. *Comput. Mater. Sci.* **1996**, *6*, 15–50.
- (65) Kresse, G.; Joubert, D. From Ultrasoft Pseudopotentials to the Projector Augmented-Wave Method. *Phys. Rev. B* **1999**, *59*, 1758–1775.
- (66) Vanderbilt, D. Berry-Phase Theory of Proper Piezoelectric Response. *J. Phys. Chem. Solids* **2000**, *61*, 147–151.